The Reconstruction of Upwind Fluxes for Conservation Laws: Its Behavior in Dynamic and Steady State Calculations

Hwajeong Choi*,[1] and Jian-Guo Liu†,[2]

Department of Mathematics, Temple University, Philadelphia, Pennsylvania 19122
E-mail: *hchoi@cims.nyu.edu and † jliu@math.temple.edu

Received May 30, 1997; revised November 11, 1997

The Euler equation of compressible flows is solved by the finite volume method, where high order accuracy is achieved by the reconstruction of each component of upwind fluxes of a flux splitting using the biased averaging procedure. Compared to the solution reconstruction in Godunov-type methods, its implementation is simple and easy, and the computational complexity is relatively low. This approach is parameter-free and requires neither a Riemann solver nor field-by-field decomposition. The numerical results from both dynamic and steady state calculations demonstrate the accuracy and robustness of this approach. Some techniques for the acceleration of the convergence to the steady state are discussed, including multigrid and multistage Runge–Kutta time methods.

Key Words: biased averaging procedure; flux splitting; finite volume method.

1. INTRODUCTION

In this paper, we consider a simple and efficient finite volume method for the Euler equation for compressible flows. The 1D system of the Euler equation is given by

$$\partial_t U + \partial_x F(U) = 0, \qquad U = \begin{bmatrix} \rho \\ m \\ E \end{bmatrix}, \qquad F = \begin{bmatrix} m \\ \rho u^2 + p \\ u(E+p) \end{bmatrix}, \tag{1.1}$$

where ρ, u, $m = \rho u$, and E are density, velocity, momentum, and total energy, respectively, and the pressure is obtained from the equation of state, $p = (\gamma - 1)(E - \rho u^2/2)$. The equation

[1] Current address: Courant Institute, New York, NY 10012.

[2] Current address: Institute for Physical Sciences and Technology, and Department of Mathematics, University of Maryland, College Park, MD 20742. Research was supported in part by NSF Grant DMS-9505275.

0021-9991/98 $25.00

in multidimensional space is given similarly. Most modern shock capturing schemes for the solution of Eq. (1.1) are of Godunov-type, which reconstructs the solution after field-by-field decomposition and solves a Riemann problem for time evolution. The well-known Godunov-type schemes are MUSCL [30], PPM [32], and ENO schemes [7, 26].

We explore an efficient implementation by using a flux splitting for the time evolution for dynamic and steady state computations. In the flux splitting, $F = F^+ + F^-$, the Jacobians of the split fluxes $F^\pm$ have only positive or negative eigenvalues. That is, each split flux always keeps only one wind direction. For this reason, they are sometimes called upwind fluxes. The high order accuracy of the scheme is achieved by directly reconstructing each component of upwind fluxes by a piecewise polynomial. Then the numerical flux in the finite volume method is determined by evaluating the reconstructed upwind fluxes on the cell boundary. We give a detailed algorithm in Section 2.

The main advantages of the flux reconstruction approach over the solution reconstruction are the simplicity of programming and computational efficiency. It is easily formulated and does not require a Riemann solver, nor does it require a characteristic decomposition or any computation for auxiliary parameters. Also, it can be easily extended to unstructured grids [4]. The Roe matrix, which is used for a characteristic decomposition, takes considerable computations in many shock capturing schemes, and in general it is difficult to find a Roe matrix for a general system of conservation laws. For instance, a Roe matrix for an MHD equation is available only for $\gamma = 2$ [2].

The flux reconstruction approach can also be found in the work of Anderson *et al.* [1], and Shu and Osher have employed an ENO procedure in reconstructing upwind fluxes of the Lax–Friedrichs splitting (LFS) after a characteristic decomposition for a system of conservation laws [26]. Another method which avoids a characteristic decomposition and solution of the Riemann problem is the central difference scheme by Nessyahu and Tadmor [21]. It achieves high resolution by using a Godunov-type method on staggered grids. Their approach can also be applied to a general systems of equations [12] and it does not require any parameters. Jin and Xin has introduced a class of relaxation schemes in [15] for multi-dimensional systems of conservation laws, based on a semilinear relaxation approximation. Their numerical results are comparable to those of the solution reconstruction approach with relatively low computational cost. Recently, X.-D. Liu and Osher proposed a convex ENO scheme for a multidimensional system of equations without using field-by-field decomposition or staggered grids [19].

In this paper, we use the newly developed biased averaging procedure (BAP) for a high order flux reconstruction [3]. The BAP finds higher order derivatives of the reconstruction without introducing spurious oscillations. Slope limiters such as van Leer or minmod limiters can also be used to determine the slope for a second order reconstruction of the upwind flux by a piecewise linear polynomial. However, the BAP is much simpler and more efficient even on unstructured grids and, unlike other slope limiters, it provides a differentiable slope [3].

For the system of gas equations, there are many other sharp and parameter-free flux splittings such as Steger–Warming splitting (SWS) [27], van Leer splitting (VLS) [29], kinetic flux vector splitting (KFVS) by Deshpande and Mandel [20], and Perthame's splitting (PS) from the first order Boltzmann scheme [23]. We have used these four splittings in our computation for both dynamic and steady state solutions. Our numerical experiments with the flux reconstruction approach show that this approach is not sensitive to the choice of flux splitting. In fact, those flux splittings behave more or less the same in the high order

flux reconstruction approach for a gas equation and their numerical results are comparable to those from the solution reconstruction approach.

It is known that many high order schemes suffer from the post-shock oscillation in the computation of slowly moving shock. Such oscillations also appear in the steady state calculations, causing slow convergence [14, 16, 24]. These post-shock oscillations can be eliminated by an entropy fix. We have studied the post-shock behavior of the flux reconstruction approach through the computation of a slowly moving shock and a steady state solution by multigrid acceleration for the flow over an airfoil. The post-shock oscillations have appeared in our computations; however, they remain relatively small compared to the result using a high order ENO scheme. We have systematically applied an entropy fix on SWS and VLS and demonstrated its effects in reducing the oscillations. Along with multigrid acceleration, we have used a three-stage Runge–Kutta time method and a special far-field boundary condition on the basis of characteristic analysis normal to the boundary, in order to accelerate the convergence in upwind-type high order methods. Also, the BAP turns out to be very effective in stabilizing the shock, resulting in faster convergence. The limiters usually work with if-statements to preserve the TVD property near extreme points, and the frequent use of if-statements sometimes causes slow convergence to steady state.

This paper is organized as follows. In Section 2, we describe the formulation of the numerical scheme with the reconstruction of fluxes for the solution of conservation laws. We also give a brief explanation as to why the reconstruction of upwind fluxes by BAP or slope limiters can be used to achieve high order accuracy. We review the flux splittings used here and describe the entropy fix for SWS and VLS in Section 3. Also, the numerical results on a wide variety of 1D and 2D model problems are presented. In Section 4, we discuss some techniques to accelerate convergence to a steady state solution, including multigrid and a three-stage Runge–Kutta time method. The computation of the steady flow over the NACA0012 airfoil using multigrid is presented as well as the quasi-1D nozzle flow using a simple time marching method. The advantage of using BAP for steady state computations will also be demonstrated.

2. FINITE VOLUME METHOD USING RECONSTRUCTIONS OF UPWIND FLUXES

In this section, we give the finite volume algorithm for the solution of conservation laws via the reconstruction of upwind fluxes of a given flux splitting using BAP. The use of the reconstruction of upwind fluxes can be understood in connection with the solution reconstruction through kinetic theory [15].

2.1. *Reconstructions of Upwind Fluxes*

We briefly describe the numerical algorithm which directly reconstructs upwind fluxes of a given flux splitting for a system of equations (1.1). We assume a uniform grid of grid size Δx. We shall use the form of conservative schemes

$$\text{(A)} \qquad U_j^{n+1} = U_j^n - \lambda(\hat{F}_{j+1/2} - \hat{F}_{j-1/2}), \qquad \lambda = \Delta t/\Delta x,$$

where U_j^n is the approximation to the cell average over the interval $(x_{j-1/2}, x_{j+1/2})$ and $\hat{F}_{j+1/2}$ is a numerical flux.

In the Godunov scheme, the numerical flux $\hat{F}_{j+1/2}$ is given by

$$\hat{F}_{j+1/2} = F(U^*(x_{j+1/2}, t)), \tag{2.1}$$

where U^* is the exact solution of a Riemann problem at $x = x_{j+1/2}$ with initial data U_j and U_{j+1} for the left- and right-hand sides of the cell boundary. A higher order extension of the scheme can be achieved by reconstructing higher order approximations to the solution and using these as a initial data for the Riemann problem. The well-known schemes using the higher order reconstruction of the solution are MUSCL, PPM, and ENO schemes. The MUSCL scheme is of second order, using a linear piecewise polynomial as an approximation, and PPM constructs the quadratic polynomial, while ENO scheme constructs an arbitrarily high order approximation by introducing a primitive function. They avoid possible oscillations near discontinuities by using limiters or adaptive stencils.

Now, we present a second order numerical scheme for conservation laws by directly reconstructing the second order approximation to each component of upwind fluxes $\hat{F}^{\pm}_{j+1/2}$ from a flux splitting, $F = F^+ + F^-$. The Jacobian of $F^{\pm}(U)$ has nonnegative eigenvalues only or nonpositive eigenvalues only. See Section 3 for a detailed discussion on various flux splittings. Let us denote by f and u a component of the flux F and the solution U, respectively. The second order reconstruction of the positive flux is obtained by a linear piecewise polynomial, $f_j^+(x)$,

(B) $$f_j^+(x) = f^+(U_j) + s_j(x - x_j), \qquad x \in (x_{j-1/2}, x_{j+1/2}).$$

In order to suppress possible spurious oscillations near discontinuities from the interpolation, we use BAP to determine the slope s_j: for the backward and forward differences, $s_l = (f^+(U_j) - f^+(U_{j-1}))/\Delta x$ and $s_r = (f^+(U_{j+1}) - f^+(U_j))/\Delta x$ of f^+ at x_j,

(C) $$s_j = \mathcal{B}^{-1}\left(\frac{\mathcal{B}(s_l) + \mathcal{B}(s_r)}{2}\right)$$

for a biased function $\mathcal{B}(x)$. Similarly, the negative flux is approximated at x_{j+1}.

The numerical flux $\hat{f}_{j+1/2}$ is then computed in a split form,

(D) $$\hat{f}_{j+1/2} = f_j^+(x)|_{x_{j+1/2}} + f_{j+1}^-(x)|_{x_{j+1/2}}.$$

Here we give some examples of the biased function, $\mathcal{B}(x)$:

(I) $\mathcal{B}(x) = \arctan(x)$, $\mathcal{B}^{-1}(x) = \tan(x)$

(II) $\mathcal{B}(x) = \tanh(x)$, $\mathcal{B}^{-1}(x) = \tanh^{-1}(x)$

(III) $\mathcal{B}(x) = \dfrac{x}{\sqrt{1+x^2}}$, $\mathcal{B}^{-1}(x) = \dfrac{x}{\sqrt{1-x^2}}$

(IV) $\mathcal{B}(x) = \dfrac{x}{\sqrt{1+x^2}+1}$, $\mathcal{B}^{-1}(x) = \dfrac{2x}{1-x^2}$

The biased average (C) plays a similar role to limiters in the second order interpolation, preventing possible oscillations near discontinuities. However, the averaging procedure gives a much easier extension to higher order approximations and to unstructured grids [3, 4]. We remark that WENO scheme [11, 18] is a similar approach to the BAP. The

WENO scheme takes a weighted convex combination of high order piecewise polynomials on all possible neighboring stencils.

Using the BAP, the flux reconstruction approach is easily extended to unstructured grids, on which the sign of the components of the exterior normal vector to a cell boundary can be used to find out the wind direction for upwind fluxes since $F^{\pm}$ is predetermined on the Cartesian coordinate system. A high order extension of the flux reconstruction follows directly from Shu and Osher's flux version ENO [26] and a high order BAP approximation [3]. As in [26], U_j represents the point value approximation of U. Then $\partial_x F^{\pm}(U_j)$ is approximated by the difference $(F^{\pm}(x_{j+1/2}) - F^{\pm}(x_{j-1/2}))/h$ and achieves high order accuracy through reconstruction of $F^{\pm}(x)$ from $F^{\pm}(u_j)$ which is viewed as a cell average of a smooth flux function.

A high order reconstruction is realized by expanding the approximate solution on a set of mean zero polynomials and using BAP to determine or limit the coefficient, as the high order solution reconstruction in [3]. Here we give an example of a third order flux reconstruction,

$$f_j^+(x) = f^+(u_j) + s_j(x - x_j) + \frac{t_j}{2}\left[(x - x_j)^2 - \frac{h^2}{12}\right], \qquad x \in (x_{j-1/2}, x_{j+1/2}), \quad (2.2)$$

where s_j is given by (C). For t_j, we consider three standard second order centered differences of $f^+(u_j)$ at x_{j-1}, x_j and x_{j+1}, denoted by t_l, t_m and t_r, respectively, and then we determine t_j by

$$t_j = \mathcal{B}^{-1}\left(\frac{1}{3}[\mathcal{B}(t_l) + \mathcal{B}(t_m) + \mathcal{B}(t_r)]\right). \quad (2.3)$$

In [3], the third order truncation error estimates for the solution reconstruction using cell averages were given, and the second and third order accuracy have also been examined for a linear convection equation with different initial data. Since two schemes coincide when cell averages are replaced by point values, we do not repeat the accuracy check here.

The BAP scheme does not have a total variation diminishing (TVD) property and it maintains a high order accuracy at extreme points. However, the second order BAP becomes a standard limiter such as minmod limiter or van Leer limiter as a scaling factor approaches zero under a certain asymptotic property of the biased function. See Lemma 2 in [3]. The BAP scheme can be viewed as a simple generalization of the limiter to high order and unstructured grid. Although we are not able to prove a total variation bounded (TVB) property for the BAP scheme, the overwhelming numerical results show that the BAP works in a stable manner. It was proved in [3] that the approximation can increase up to at most $O(h)$ at extreme points and this enables us to show that the approximate solution is indeed bounded for the scalar case.

Before we present numerical behavior of the above scheme, we would like to briefly mention why the reconstruction of upwind fluxes is a plausible approach. The flux splittings originate from the kinetic approach to conservation laws [20, 23]. The earlier work on the kinetic approach dates back to Sanders and Prendergast [25]. Lax *et al.* have studied the connection between Steger–Warming flux splitting and Boltzmann schemes [8]. We revisit the relaxation scheme of Jin and Xin, who show that the reconstruction of the variable of the kinetic equation boils down to the reconstruction of the upwind flux vectors of the Lax–Friedrichs splitting [13, 15]. Their scheme is called a relaxed scheme when $\epsilon = 0$.

The 1D conservation law

$$\partial_t U + \partial_x F(U) = 0 \tag{2.4}$$

is approximated by a Jin–Xin relaxation system

$$\begin{aligned} \partial_t U + \partial_x V &= 0 \\ \partial_t V + A^2 \partial_x U &= \frac{1}{\epsilon}(F(U) - V), \end{aligned} \tag{2.5}$$

where A is a constant diagonal matrix satisfying the subcharacteristic condition [15] and the diagonalized system of (2.5) is given by

$$\partial_t W^{\pm} \pm A \partial_x W^{\pm} = \frac{1}{\epsilon}(F(U) - V), \tag{2.6}$$

where

$$W^{\pm} = \frac{1}{2}(V \pm AU). \tag{2.7}$$

At the zero limit of ϵ, the flux variable V is relaxed to equilibrium state $F(U)$, i.e.,

$$V \sim F(U) \qquad \text{as } \epsilon \to 0. \tag{2.8}$$

From (2.8) together with (2.7), one has

$$W^{\pm} \sim \frac{1}{2}(F(U) \pm AU) \equiv F^{\pm}(U). \tag{2.9}$$

Note that $F^{\pm}$ in (2.9) is a Lax–Friedrichs flux splitting, $F(U) = F^{+}(U) + F^{-}(U)$.

The diagonalized system (2.6) with the fixed wave direction specified by $\pm A$ can be solved easily by any upwind type scheme and one can achieve high resolution by directly reconstructing the variable $W^{\pm}$ in high order. When the method of lines is applied to (2.6), the upwind scheme gives

$$\partial_t W^{+}(x_j) + A\frac{1}{\Delta x}(W^{+}(x^{-}_{j+1/2}) - W^{+}(x^{-}_{j-1/2})) = \frac{1}{\epsilon}(F(U_j) - V_j) \tag{2.10}$$

$$\partial_t W^{-}(x_j) - A\frac{1}{\Delta x}(W^{-}(x^{+}_{j+1/2}) - W^{-}(x^{+}_{j-1/2})) = \frac{1}{\epsilon}(F(U_j) - V_j). \tag{2.11}$$

Since the variable U is written in $W^{\pm}$, $U = A^{-1}(W^{+} - W^{-})$. Multiplying by A^{-1} after subtracting (2.11) from (2.10), one has

$$\partial_t U_j + \frac{1}{\Delta x}(W^{+}(x^{-}_{j+1/2}) - W^{+}(x^{-}_{j-1/2})) + \frac{1}{\Delta x}(W^{-}(x^{+}_{j+1/2}) - W^{-}(x^{+}_{j-1/2})) = 0. \tag{2.12}$$

As $\epsilon \to 0$, with (2.9) the upwind scheme in (2.12) becomes

$$\partial_t U_j + \frac{1}{\Delta x}(F^{+}_{j+1/2-0} - F^{+}_{j-1/2-0}) + \frac{1}{\Delta x}(F^{-}_{j+1/2+0} - F^{-}_{j-1/2+0}) = 0 \tag{2.13}$$

where $F^{+}_{j\pm1/2-0} = F(U(x^{-}_{j\pm1/2}))$ and $F^{-}_{j\pm1/2+0} = F(U(x^{+}_{j\pm1/2}))$. This shows that using BAP or slope limiters in the reconstruction of variable $W^{\pm}$ in MUSCL-type schemes for system (2.6) is equivalent to using them directly on the flux vectors $F^{\pm}$ in (2.9) at the zero limit of ϵ.

3. FLUX SPLITTING AND ENTROPY FIX

Many different flux splittings have been developed in the past decade, and their development is still an active research area [17]. We have considered four representative flux splittings to implement the finite volume method via the reconstruction of the upwind fluxes of a flux splitting using BAP. They are Steger–Warming splitting [27], van Leer splitting [29], kinetic flux vector splitting [20] by Mandel and Deshpande, and Pertham's flux splitting from his Boltzmann-type schemes [23]. We have conducted some numerical experiments with a LFS in (2.9) which is used in the relaxed schemes and flux version ENO schemes. The choice of the diagonal matrix A is problem dependent and thus we prefer to present the numerical results with more robust and parameter-free flux splittings for a gas equation, such as SWS, VLS, KFVS, and PS.

During the course of numerical experiments, we have encountered the same problems that many modern shock capturing schemes have, such as downstream oscillation in slowly moving shock and nonphysical behavior near the corner of the step in the computation of the Mach 3 flow in a tunnel with a step. These problems as well as the slow convergence to steady state solutions are known to be caused by the unsteady viscosity profile [14, 16, 24]. They often occur when the amount of numerical dissipation keeps varying and sometimes almost vanishes near sonic points. The typical cure for these is an entropy fix which allows more numerical dissipation to avoid nearly zero viscosity in the vicinity of sonic points [16]. The numerical results with an entropy fix will be presented later in this section.

(i) *Steger–Warming splitting.* SWS has been obtained by a similarity transformation on the flux vector using the property, $F(U) = A(U)U$, $A(U) = F'(U)$, due to the fact that the flux vector is a homogeneous function of degree one. The flux splitting of F in (1.1) is given by

$$F(U) = F^+(U) + F^-(U) = Q^{-1}\Lambda^+ QU + Q^{-1}\Lambda^- QU, \tag{3.1}$$

where $A = Q^{-1}\Lambda Q$ and $\Lambda^\pm = diag(\lambda_1^\pm, \lambda_2^\pm, \lambda_3^\pm)$, $\lambda_i^\pm = (\lambda_i \pm |\lambda_i|)/2$, $i = 1, 2, 3$.

The Steger–Warming splitting can be explicitly expressed in terms of eigenvalues of the Jacobian of F, $\lambda_1 = u$, $\lambda_2 = u + c$, and $\lambda_3 = u - c$,

$$F_{\mathrm{SWS}}^\pm = \frac{\rho}{2\gamma}\begin{pmatrix} 2(\gamma-1)\lambda_1^\pm + \lambda_2^\pm + \lambda_3^\pm \\ 2(\gamma-1)\lambda_1^\pm u + \lambda_2^\pm(u+c) + \lambda_3^\pm(u-c) \\ (\gamma-1)\lambda_1^\pm u^2 + \frac{1}{2}\lambda_2^\pm(u+c)^2 + \frac{1}{2}\lambda_3^\pm(u-c)^2 + W \end{pmatrix}, \tag{3.2}$$

where

$$W = \frac{(3-\gamma)(\lambda_2+\lambda_3)c^2}{2(\gamma-1)} \tag{3.3}$$

and c is the local speed of sound. Artificial viscosity can be easily introduced into SWS by simply adding a small positive (or negative) number to $\lambda_i^\pm$. The new eigenvalues, $\tilde{\lambda}_i^\pm$,

$$\tilde{\lambda}_i^\pm = \frac{\lambda_i \pm \left(\lambda_i^2 + \epsilon^2\right)^{1/2}}{2} \tag{3.4}$$

can be used for a smooth transition through the sonic points [1].

(*ii*) *Van Leer splitting*. Van Leer has developed a splitting in terms of the local Mach number M, $M = u/c$, which is differentiable even at sonic points. For $M \geq 1$, the eigenvalues of the Jacobian of F are all positive and thus the positive flux F^+_{VLS} is F itself and the negative flux, $F^-_{\mathrm{VLS}} = 0$. Similarly, $F^+_{\mathrm{VLS}} = 0$ and $F^-_{\mathrm{VLS}} = F$ for $M \leq -1$. The van Leer splitting is given as follows for $-1 < M < 1$,

$$F^{\pm}_{\mathrm{VLS}} = \begin{pmatrix} f_1^{\pm} \\ f_1^{\pm} \frac{(\gamma-1)u \pm 2c}{\gamma} \\ f_1^{\pm} \frac{((\gamma-1)u \pm 2c)^2}{2(\gamma^2-1)} \end{pmatrix}, \tag{3.5}$$

where $f_1^{\pm} = \pm \rho c (M \pm 1)^2/4$. The Jacobian of the positive flux $(F^+_{\mathrm{VLS}})'$ has two positive eigenvalues and one zero eigenvalue, while $(F^-_{\mathrm{VLS}})'$ has two negative eigenvalues and one zero eigenvalue.

Unlike SWS, it is not clear how to impose artificial viscosity on the split fluxes of the van Leer splitting. For the entropy fix, we have tried to avoid zero or small eigenvalues by adding an extra term to each component of $F^{\pm}_{\mathrm{VLS}}$. The following splitting, $\tilde{F}^{\pm}_{\mathrm{VLS}}$, has been used for the entropy fix in our computations,

$$\tilde{F}^{\pm}_{\mathrm{VLS}} = F^{\pm}_{\mathrm{VLS}} \pm \alpha \begin{pmatrix} \rho c \\ \rho c \frac{(\gamma-1)u}{\gamma} \\ \beta \rho c^3 \frac{1}{2(\gamma^2-1)} \end{pmatrix} \tag{3.6}$$

for some $\alpha, \beta > 0$. Although the closed form for the eigenvalues of $\tilde{F}^{\pm}_{\mathrm{VLS}}$ is not available, the traces of the Jacobians of both positive and negative fluxes are increased in absolute value for $1 \leq \gamma \leq 3$. Numerical results clearly show the effect of artificial viscosity of the augmented terms. We note that in our numerical experiments both SWS and VLS show quite satisfactory results, although VLS shows more robust behavior overall.

(*iii*) *Kinetic flux vector splitting* and *Perthame's flux splitting*. The KFVS, by Mandel and Deshpande [20], and Perthame's flux splittings [23] have been motivated by the fact that the Euler equation can be derived from the moment closure of a Boltzmann-like equation for equilibrium gas.

Deshpande and Mandel have formulated their flux splitting from the following moment form of Boltzmann-like equation for the inviscid gas equation,

$$\langle \psi, \partial_t f + \xi \cdot \nabla_x f \rangle = 0, \tag{3.7}$$

$$f(t, x, \xi, I) = \frac{\rho}{I_0 (2\pi RT)^{N/2}} \exp\left(-\frac{|\xi - u|^2}{2RT} - \frac{I}{I_0} \right), \tag{3.8}$$

where ψ is a collisional invariant given by

$$\psi = (1, \xi, I + |\xi|/2),$$

ξ is the velocity of particle, I is an internal energy variable, and I_0 is a normalizing constant

for internal energy. For a polytropic gas with γ as the ratio of specific heats, $I_0 = ((3-\gamma)/2(\gamma-1))RT$. Density, momentum, and total energy are related to f by

$$\langle \psi, f \rangle = (\rho, \rho u, E),$$

and T is the temperature determined by Boyle's law $T = p/(R\rho)$ for prefect gas. The flux splitting has been obtained by the moment closure of (3.7) over the positive and negative speed of particles.

A similar approach is proposed by Perthame in [23] with a square-shaped distribution function, which has a compact support. His flux splitting is also obtained through the moment closure of a linear transport equation over the positive and negative speed of the particles. While the first order Boltzmann scheme gives rise to a flux splitting, his second order scheme is obtained through the second order reconstruction of a distribution function. The second order Boltzmann scheme is rather complicated, requiring relatively heavy computations, and does not have a simple extension to 2D problems. In the flux reconstruction approach, the flux splitting from his first order scheme is only needed since the second order accuracy is achieved through the reconstruction of the split fluxes.

Now we present some numerical results with these flux splittings via the reconstruction of the upwind fluxes. More test problems follow in the next section. The extensive numerical experiments show that in spite of their different derivations, these flux splittings behave more or less the same for the high order flux reconstruction approach, indeed showing quite satisfactory performance on every test problem. Although we have not used splittings other than the aforementioned ones, similar behavior is expected from other flux splittings. We have omitted some results if they have little difference from the one shown here and denote by BAP-2-FS and BAP-3-FS the second and the third order BAP scheme using a flux splitting, FS, respectively.

We have had quite good numerical results for most of the test problems without any fix. However, when SWS or VLS is used for the computation of the flow in a tunnel with a step, an expansion shock has been developed near the corner of the step, as can be seen in Fig. 5. The downstream oscillations in a slowly moving shock also appeared in our computations, although the oscillations are relatively small compared to high order ENO schemes [26]. These nonphysical behaviors have been eliminated by the entropy fix given in (3.4) for SWS and (3.6) for VLS. KFVS and PS seem more dissipative than SWS or VLS. They did not show any nonphysical behavior for any of the test problems. Although the oscillations are still followed by the slowly moving shock, they are almost negligible.

EXAMPLE 1 (TWO INTERACTING BLAST WAVE [32]). The initial data are

$$\rho = 1, u = 0 \qquad \text{for } 0 \le x \le 1,$$
$$p = 1000 \text{ for } 0 \le x \le 0.1; \qquad 0.01 \text{ for } 0.1 < x \le 0.9; \qquad 100 \text{ for } 0.9 < x \le 1.$$

We have used 400 grid points to compute the numerical solution at $t = 0.03$ and $t = 0.038$ with $\Delta t = 0.00002$. The solution has quite complex structure. The results in Figs. 1 and 2 show that most of features are well captured. The results from the second order Boltzmann scheme are also presented for comparison. It shows slightly better performance near the shock in the densities. The third order results using (2.2) are shown in Fig. 3.

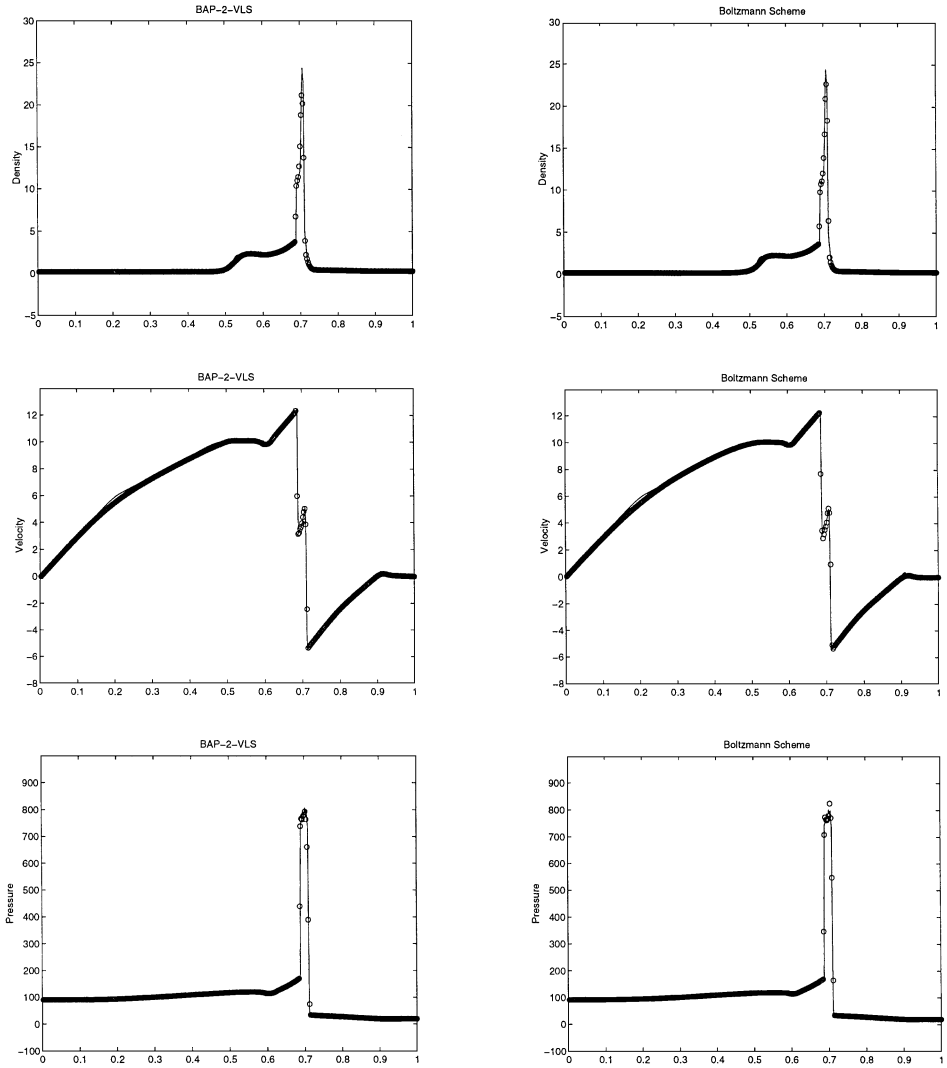

FIG. 1. Two interacting blast wave, 400 points at $t = 0.03$. Left: BAP-2-VLS. Right: Second order Boltzmann scheme. From top to bottom: density, velocity, and pressure.

EXAMPLE 2 (SLOWLY MOVING SHOCK [24]). The initial data are taken by

$$U_L = \begin{bmatrix} 3.86 \\ -3.1266 \\ 27.0913 \end{bmatrix} \text{ if } 0 \le x < 0.5, \qquad U_R = \begin{bmatrix} 1 \\ -3.44 \\ 8.4168 \end{bmatrix} \text{ if } 0.5 \le x \le 1. \tag{3.9}$$

The speed of the shock is 0.1096. We have used 100 grid points with $\Delta t = 0.001$. Figure 4 shows the densities at $t = 0.95$ computed by BAP-2-VLS with and without an entropy fix. Even without an entropy fix, the oscillations behind the shock are quite small compared to those for the third order ENO scheme. For comparison we also show densities computed by BAP-2-KFVS and BAP-2-PS in Fig. 4. No fix is added to KFVS nor PS. The oscillations in the solution by KFVS are almost negligible.

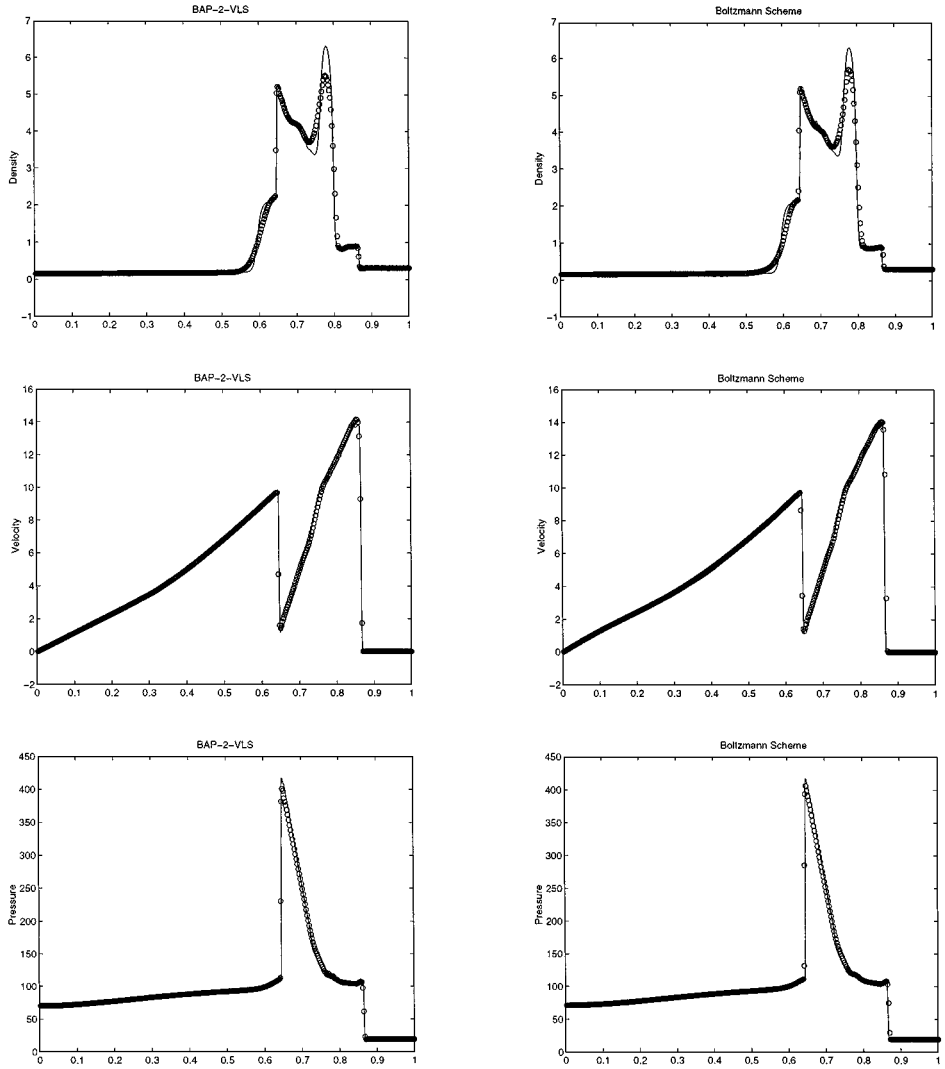

FIG. 2. Same as Fig. 1, for $t = 0.038$.

EXAMPLE 3 (MACH 3 WIND TUNNEL WITH A STEP [32]). The wind tunnel is 1 length unit wide and 3 length units long with a step of 0.2 length unit high, located 0.6 length unit from the left end of the tunnel. The tunnel is initialized by a gamma-law gas going from left to right, which has density 1.4, pressure 1.0, and velocity 3.0. The initial state of the gas is also used at the left-hand boundary. At the right-hand boundary, all gradients are set to zero. The reflecting boundary condition is used at the walls of the tunnel.

We have used a uniform grid of the size 240×80 with $\Delta x = \Delta y = \frac{1}{80}$. Thirty equally spaced density contours at $T = 4$ are shown in Fig. 5. Without an entropy fix, the VLS has developed an expansion shock near the corner as can be seen in the first image in Fig. 5. Such nonphysical behavior has been treated by using the fluxes, $\tilde{F}^{\pm}_{\mathrm{VLS}}$, in the small region around the corners. While SWS shows the same behavior as VLS, the other two, KFVS and PS, work well without any fix. The density contour from BAP-2-KFVS is also shown in Fig. 5.

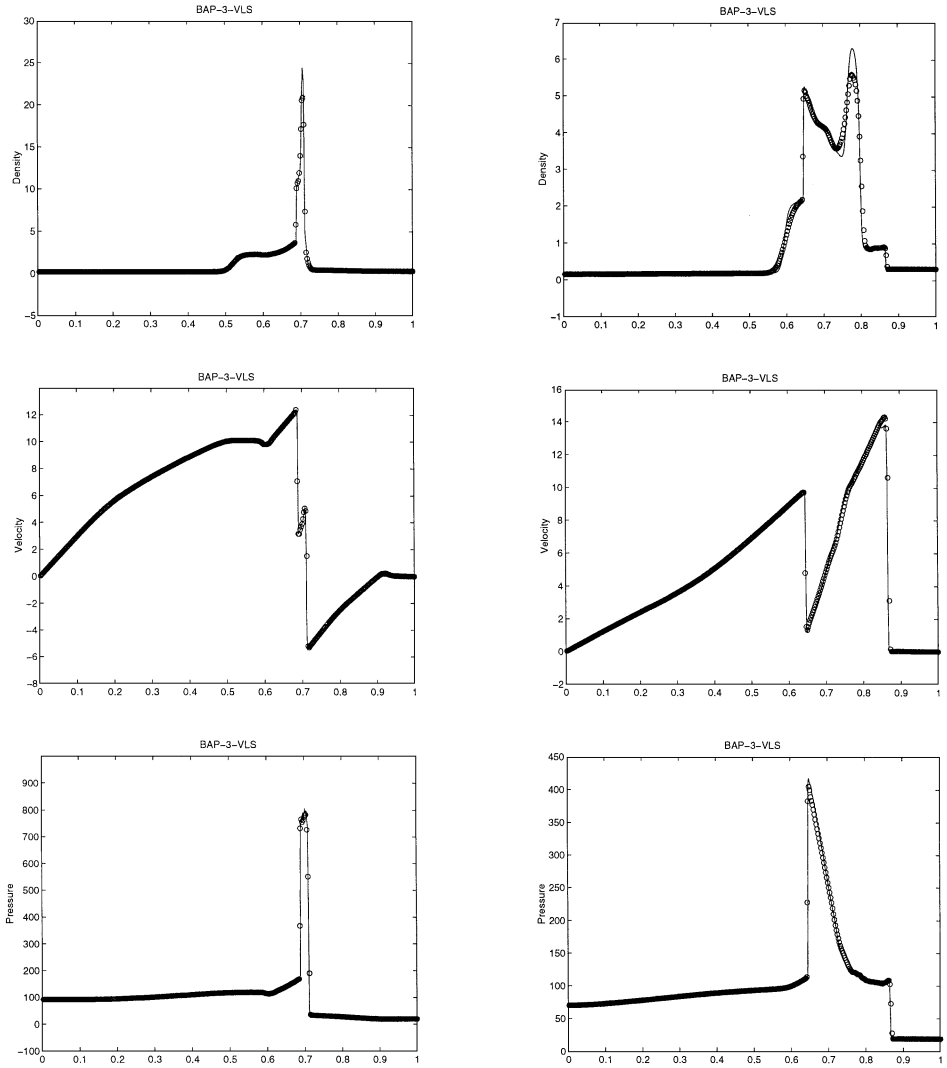

FIG. 3. Two interacting blast wave computed by BAP-3-VLS on 400 points. Left: $t = 0.03$. Right: $t = 0.038$. From top to bottom: density, velocity, and pressure.

EXAMPLE 4 (FLOW PAST A CYLINDER). A steady flow past a cylinder at a freestream Mach number of 3.0 has been computed. The domain is an annular region with a circle of radius 1.0 as an inner boundary and a circle of radius 11.0 as an outer boundary. The grid in the angular direction is distributed uniformly, while in the radial direction it is nonuniform. We have used a grid of size 180×50.

This problem is known to be difficult to compute because the region of very low pressure and low density develops at the rear of the cylinder. In such regions, negative densities and pressure appeared during the calculations, which breaks down most numerical schemes. We have also encountered this difficulty. In order to stabilize such regions we have added artificial viscosity to the small rectangular region behind the cylinder. The amount of artificial viscosity is smoothly varied, having zero artificial viscosity on the boundary of the rectangular region.

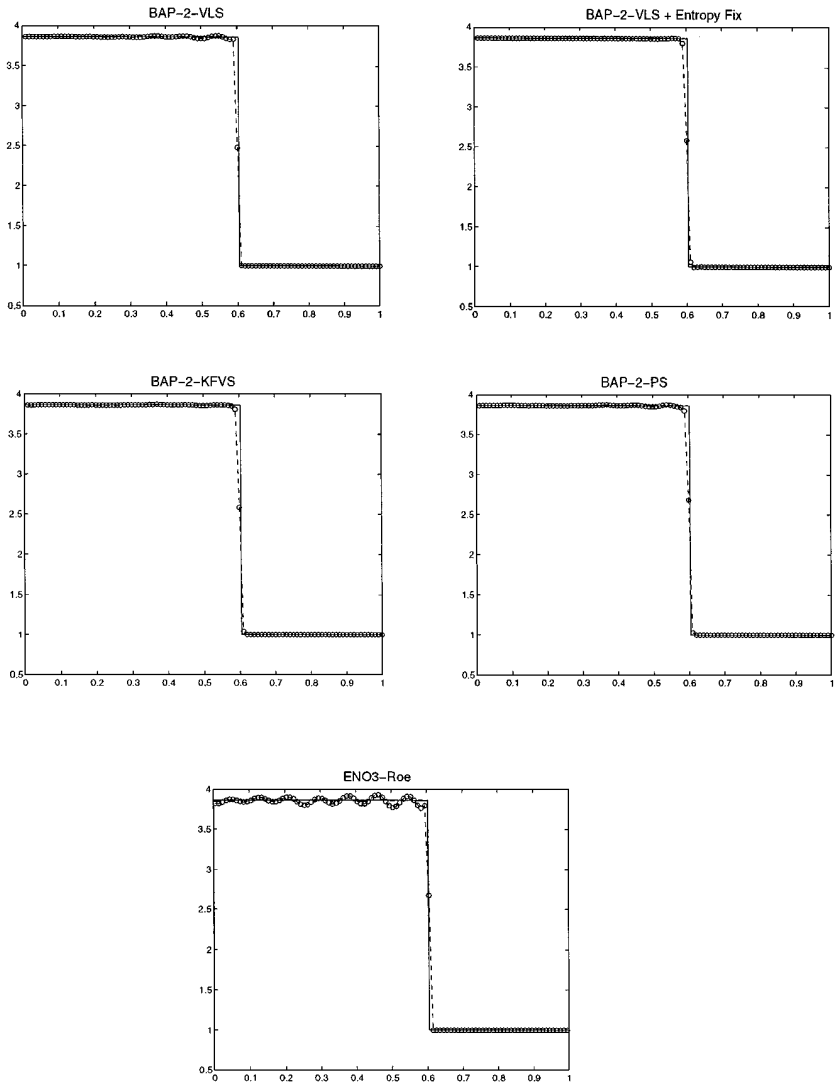

FIG. 4. Slowly moving shock problem, densities at $t = 0.95$ on 100 points. From left to right, top to bottom: BAP-2-VLS, BAP-2-VLS + entropy fix, BAP-2-KFVS, BAP-2-PS, and the third order ENO scheme.

The results at $T = 6$ using VLS and KFVS are shown in Fig. 6. The other two splittings show similar results. Mach number contours with 25 equally spaced levels are presented. The solid line is the result on a grid 360×100. Both the sharp bow shock in the front, and a V-shaped weak shock behind the cylinder are fairly well captured. The Mach number distribution along the symmetry line and over the cylinder is also shown, which indicates the sharp shock profile and the acceleration over the cylinder very well. Even with artificial viscosity added to the rear of the cylinder the results are much sharper than the one given in [5].

4. STEADY STATE CALCULATIONS

We have also computed the steady state solution of 1D nozzle flow and the flow over an airfoil in order to show convergence behavior of the flux reconstruction algorithm with

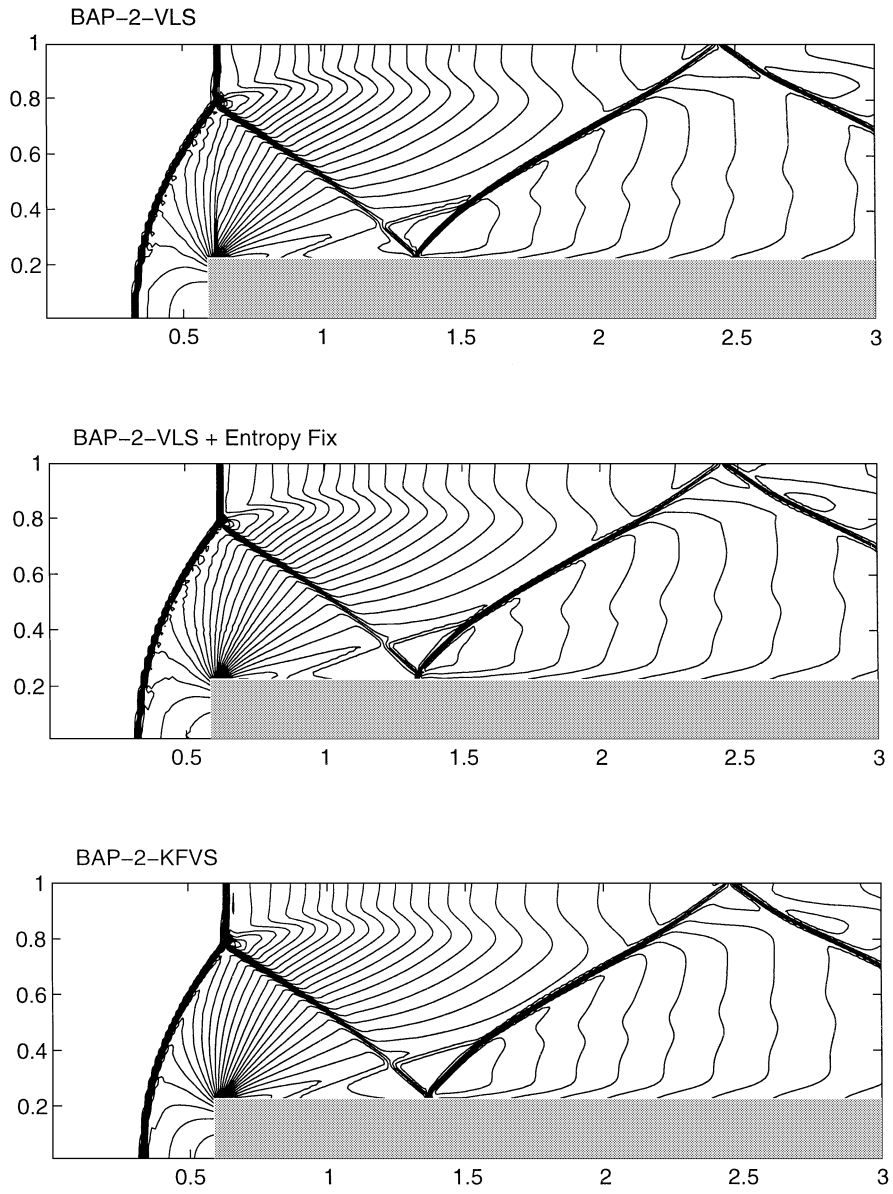

FIG. 5. Mach 3 flow in a tunnel with a step. Density contours at $T = 4$. Grid 240×80. From top to bottom: BAP-2-VLS, BAP-2-VLS + entropy fix, and BAP-2-KFVS. The expansion shock near the corner typically appears in many different schemes. It is avoided by an entropy fix.

a biased averaging procedure in both time marching and multigrid acceleration. Several well-known techniques have been employed to accelerate the convergence of the flow over an airfoil, such as multigrid, multistage time method, local time stepping, and a special treatment for far-field boundary conditions.

4.1. *Time Marching*

We have computed the steady state solution of the quasi-1D nozzle flow by BAP-2-VLS using a simple time marching method and compared it with the third order ENO scheme [26].

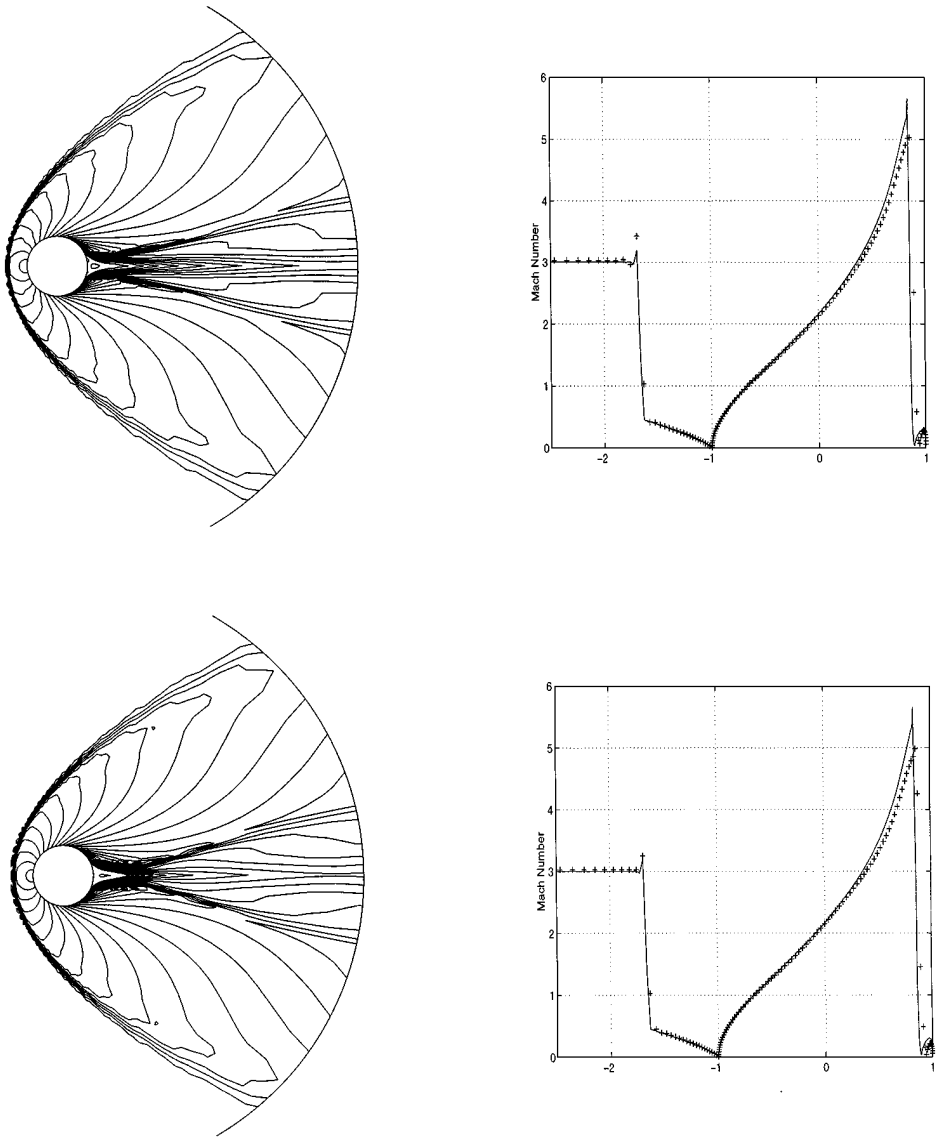

FIG. 6. Flow over a cylinder. Mach $=3.0$ at $T=6$. Grid 180×50. Left: Mach number contour. Right: Mach numbers on the symmetry line and over the cylinder. Top: BAP-2-VLS. Bottom: BAP-2-KFVS.

We consider a divergent nozzle with the area $k(x)=1.398+0.347\tanh(0.8x-4)$ [6]. The Euler equations describing the quasi-1D nozzle flow are

$$\partial_t(\rho k)+\partial_x(mk)=0, \tag{4.1}$$

$$\partial_t(mk)+\partial_x(\rho u^2k+pk)=p\partial_x k, \tag{4.2}$$

$$\partial_t(Ek)+\partial_x(u(E+p)k)=0. \tag{4.3}$$

The steady state solution has supersonic inflow and subsonic outflow. We have used 50 points on the computational domain, $0\le x\le 10$. A linear interpolation between the exact steady state boundary values is used as the initial condition, and the boundary condition at

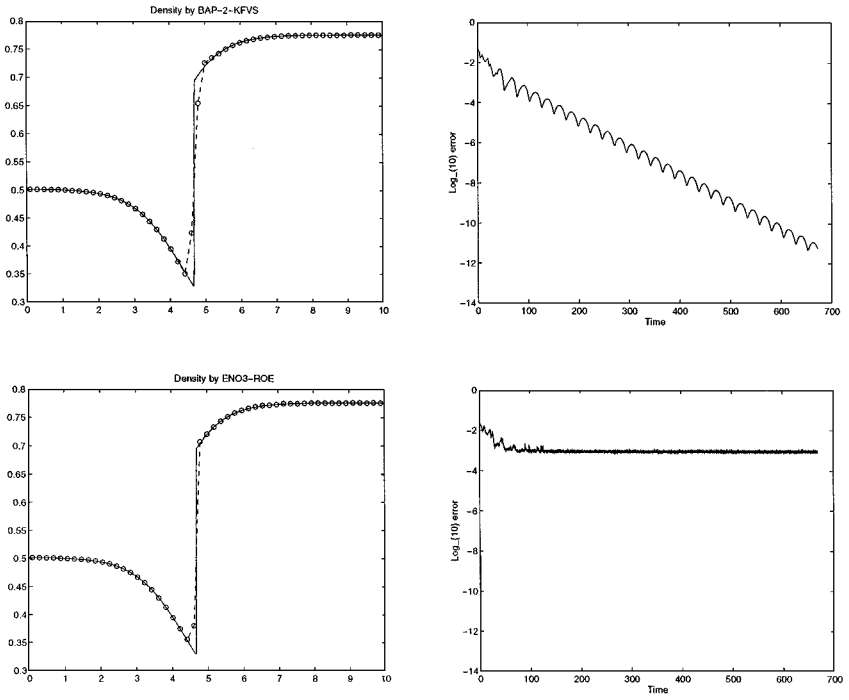

FIG. 7. Steady state solution of quasi-1D nozzle flow, density, and convergence history. Top: BAP-2-KFVS. Bottom: Third order ENO scheme.

$x = 0$ is specified by $(\rho k, mk, Ek)(0, t) = (0.5277, 0.6855, 1.4465)$. For the right boundary at $x = 10$, ρk is given by $(\rho k)(10, t) = 3.4540$ and extrapolation is used to determine the other two variables.

In Fig. 7, we show the results from the flux reconstruction approach using KFVS and the third order ENO scheme. The log plots of errors are shown in the right column of the figure to compare the convergence. The flux version approach using the BAP gives relatively faster convergence, while the ENO scheme stagnates after a certain time. The slow convergence of the ENO scheme for 1D nozzle flow was also discussed in [14]. The WENO, which has a concept similar to that of BAP, also shows a faster convergence for this problem [11].

4.2. *Multigrid*

Multigrid methods provide a faster convergence by reducing the high frequency of the residual corresponding to each different level of the grids. Multigrid can be considered the way to reach the steady state using a dynamic approach on hierarchical grids. For instance, in the multigrid method for a Poisson equation on a square, the weighted Jacobi iteration is indeed the same as the forward Euler time discretization of a heat equation, whose CFL number is chosen to be $1/3$. We have considered $\Delta t/\Delta x^2$ as a CFL number for a heat equation, while for the convection–diffusion problem, we refer CFL number to the maximum of standard CFL number $u\Delta t/\Delta x$ and $\mu\Delta t/\Delta x^2$ where u is the convection speed and μ is the diffusion coefficient.

The use of multigrid for time-dependent problem allows large time steps on coarse grids so that disturbances are more rapidly expelled through the outer boundary. We have used

the explicit multigrid method of Jameson [10] with the BAP-2-VLS on each grid level. For a time discretization, the multistage time methods have been largely used to increase the CFL number by extending the stability region. For example, for a convection-dominated problem such as the flow over an airfoil which has eigenvalues on the imaginary axis, Jameson [10] has developed a multistage time method whose stability region includes eigenvalues on the imaginary axis. His five-stage method is known to be very effective in a centered difference scheme with artificial dissipations. However, problem-dependent fine tuning is sometimes needed when combining artificial dissipation, and the resulting shock profiles are not as sharp as the upwind-type methods. We have used a three-stage Runge–Kutta method of the form for an ordinary differential equation $u_t = L(u)$ at the $(n+1)$th time step,

$$\begin{aligned} u^{(1)} &= u^n + \alpha_1 \Delta t L(u^n) \\ u^{(2)} &= u^n + \alpha_2 \Delta t L\left(u^{(1)}\right) \\ u^{n+1} &= u^n + \Delta t L\left(u^{(2)}\right), \end{aligned} \tag{4.4}$$

with $\alpha_1 = \alpha_2 = 1/2$. The important feature of this time stepping method is that its stability region takes the largest part of the imaginary axis among all other three-stage time stepping methods. It also minimizes the required memory space in the implementation since it consists of three forward Euler time steps. We note that this three-stage method is of second order. However, the time accuracy is not important in steady state calculations. In Fig. 8, we compare the stability regions of the optimal three-stage method (4.4) with $\alpha_1 = \alpha_2 = 1/2$ with the standard three-stage time method with $\alpha_1 = 1/3$ and $\alpha_2 = 1/2$.

Another useful time stepping to accelerate the convergence, especially for a nonuniform grid, is the local time stepping which allows maximum local CFL number determined by the local stability analysis [10]. Other difficulties in steady state calculations of the flow over an airfoil arise from the post-shock oscillations and the far-field boundary condition. The post-shock oscillations and inappropriate far-field boundary condition are known to trigger slow convergence. To reduce the post-shock oscillations, we have tried the entropy fix as given in Section 3 and found it to be effective in accelerating the convergence. We note that

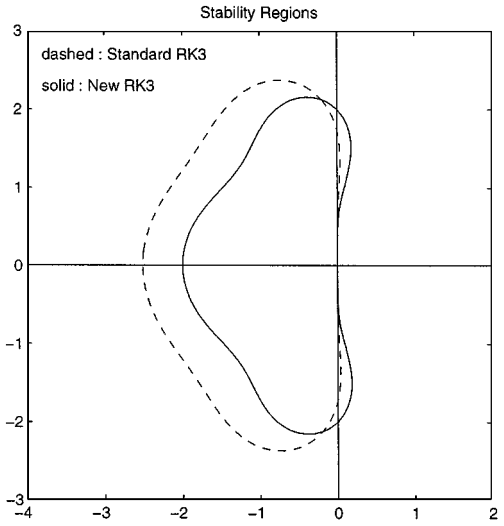

FIG. 8. Stability regions of the Runge–Kutta time method.

fewer post-shock oscillations occur with BAP than with other slope limiters. Slope limiters generally employ if-statements to preserve their TVD property by setting the averaged slope to be zero near extreme points. The if-statements result in nondifferentiability of the limiters and they are often sensitive to small perturbations, causing slow convergence. The biased averaging procedure uses one smooth function as a biased function and thus it seems less disturbing to the shock when the solution gets close to convergence. For the treatment of the far-field boundary condition, we have used the one in [10, 28], which is based on characteristic analysis on the one-dimensional isentropic flow normal to the boundary. The circulation is added for the computation on a relatively small domain.

EXAMPLE 5 (FLOW OVER NACA0012 AIRFOIL). We show the results from the steady state transonic flow calculations for the NACA0012 airfoil. The computation has been done on a 160×32 grid, as shown in Fig. 9. As described above, multigrid with three-stage time method (4.4), as well as the local time stepping, has been used for the acceleration of the convergence.

The results with the initial Mach number 0.8 and the angle of attack 1.25° are shown in Fig. 9. We have tested minmod and van Leer limiters in the same multigrid algorithm. As can

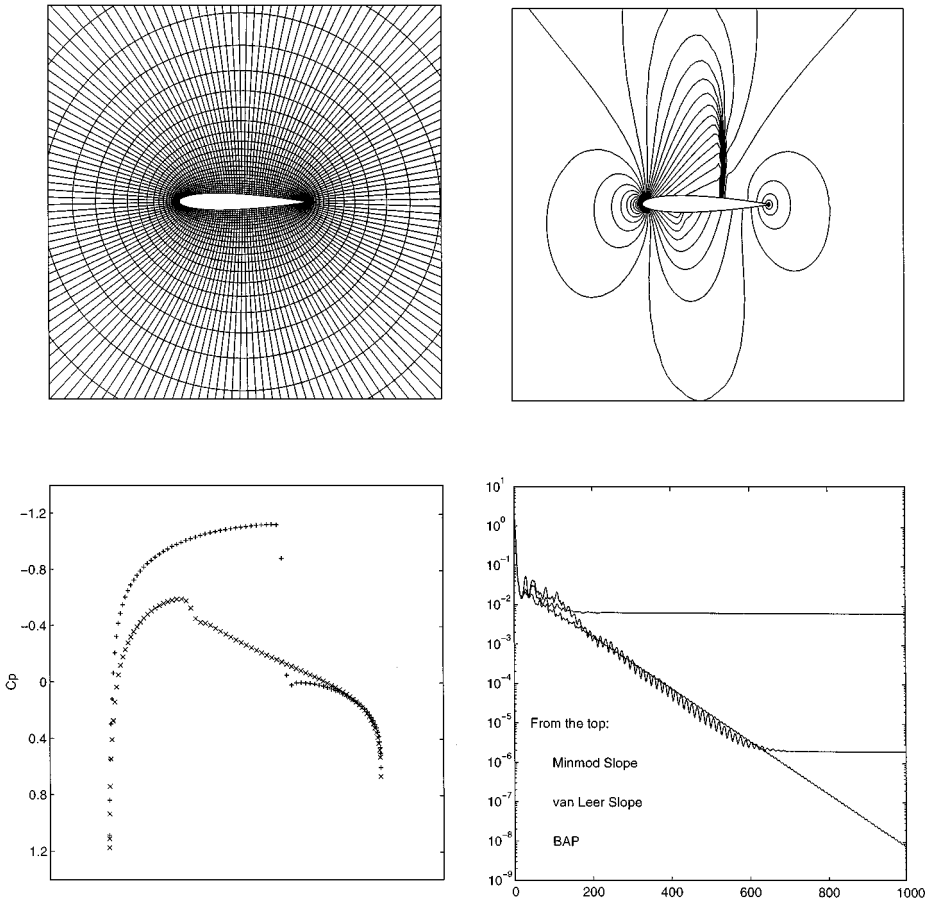

FIG. 9. Flow over a NACA0012 airfoil by BAP-2-VLS, for $M = 0.8$ and $\alpha = 1.25^\circ$. Top left: Grid 160×32. Top right: Mach contour. Bottom left: Pressure coefficient. Bottom right: Convergence history.

be seen in the convergence history in Fig. 9, both the minmod limiter and van Leer limiter stagnate the convergence, while the residual keeps decreasing with the biased averaging procedure. This clearly demonstrates the robustness of the biased averaging procedure in steady state calculations. The convergence can be accelerated even further with an entropy fix. The slow convergence due to the limiters on unstructured grids was discussed in [31].

5. CONCLUSIONS

The robustness and accuracy of the componentwise flux reconstruction approach, the construction of approximations to upwind fluxes using the BAP, have been demonstrated in this paper, through a wide variety of test problems in dynamic and steady state calculations. No Riemann problem nor characteristic decomposition is involved in this approach and therefore, its programming is simple and the computational complexity is much lower than the Godunov-type methods which use the solution reconstruction.

As can be seen in steady state calculations, both BAP and flux splitting are less sensitive to perturbations, resulting in faster convergence compared to slope limiters and characteristic decomposition by a Roe matrix. We have tried a systematic entropy fix to eliminate postshock oscillations and found it to be very useful in accelerating the convergence of the solution to steady state.

ACKNOWLEDGMENTS

This work has benefited from many stimulating discussions with Shi Jin, Stanley Osher, Chi-Wang Shu, and Zhouping Xin. We thank Bjorn Engquist and Smadar Karni for bringing to our attention the steady state problems.

REFERENCES

1. W. Anderson, J. Thomas, and B. van Leer, Comparison of finite volume flux vector splittings for the Euler equations, *AIAA J.* **24**, 1453 (1986).
2. M. Brio and C. C. Wu, An upwind difference scheme for the equations of ideal magnetohydrodynamics, *J. Comput. Phys*. **75**, 400 (1988).
3. H. Choi and J.-G. Liu, *Shock capturing with a simple biased averaging procedure*, submitted for publication.
4. H. Choi, *Robust Numerical Methods for Conservation Laws Using a Biased Averaging Procedure*, Ph.D. dissertation, Temple University (1997).
5. A. Dervieux, B. van Leer, J. Periaux, and A. Rizzi, *Numerical Simulation of Compressible Euler Flows*, Notes on Numerical Fluid Mechanics, Vol. 26 (Vieweg and Sohn, Wicsbaden, 1989).
6. H. Glaz and T.-P. Liu, The asymptotic analysis of wave interactions and numerical calculations of transonic nozzle flow, *Adv. Appl. Math*. **5**, 111 (1984).
7. A. Harten, B. Engquist, S. Osher, and S. Chakravarthy, Uniformly non-oscillatory schemes, III, *J. Comput. Phys*. **71**, 231 (1987).
8. A Harten, P. Lax, and B. van Leer, On upstream differencing and Godunov-type schemes for hyperbolic conservation laws, *SIAM Rev*. **25**, 35 (1983).
9. A. Jameson and P. D. Lax, *Conditions for the Construction of Multi-point Total Variation Diminishing Difference Schemes*, Princeton University Report MAE 1650 (1984).
10. A. Jameson, W. Schmidt, and E. Turkel, *Numerical solutions of inviscid transonic flow over a complete aircraft, AIAA Paper 81-1259* (Jan. 1981).
11. G. Jiang and C.-W. Shu, Efficient implementation of weighted ENO schemes, *J. Comput. Phys*. **126**, 202 (1996).

12. G. Jiang and E. Tadmor, Nonoscillatory central schemes for multidimensional hyperbolic conservation laws, *SIAM J. Sci. Comput*. (to appear).
13. S. Jin, Numerical integrations of systems of conservation laws of mixed type, *SIAM J. Appl. Math.* **55**, 1536 (1995).
14. S. Jin and J.-G. Liu, The effects of numerical viscosities. I. Slowly moving shocks, *J. Comput. Phys*. **126**, 373 (1996).
15. S. Jin and Z. Xin, The relaxation schemes for systems of conservation laws in arbitrary space dimensions, *Comm. Pure Appl. Math.* **55**, 235 (1995).
16. S. Karni and S. Čanić, Computations of slowly moving shocks, *J. Comput. Phys*. **136**, 132 (1997).
17. M.-S. Liou and C. J. Steffen, A new flux splitting scheme, *J. Comput. Phys*. **107**, 23 (1993).
18. X-D. Liu, S. Osher, and T. Chan, Weighted essentially non-oscillatory schemes, *J. Comput. Phys*. **115**, 200 (1994).
19. X-D. Liu and S. Osher, *Convex ENO high order multidimensional schemes without field by field decomposition or staggered grids*, preprint.
20. J. Mandel and S. Deshpande, Kinetic flux vector splitting for Euler equations, *Comp. Fluids* **23**, 447 (1994).
21. H. Nessyahu and E. Tadmor, Non-oscillatory central differencing for hyperbolic conservation laws, *J. Comput. Phys*. **87**, 408 (1990).
22. S. Osher and F. Solomon, Upwind difference schemes for hyperbolic systems of conservation laws, *Math. Comp*. **38**, 339 (1982).
23. B. Perthame, Second order Boltzmann schemes for compressible Euler equations in one and two space dimensions, *SIAM J. Numer. Anal*. **29**, 1 (1992).
24. J. Quirk, A contribution to the great Riemann solver debate, *Int. J. Numer. Methods Fluids* **18**, 555 (1994).
25. R. Sanders and K. Prendergast, The possible relation of the three-kiloparsec arm to explosions in the galactic nucleus, *Astrophys. J*. **188** (1974).
26. C.-W. Shu and S. Osher, Efficient implementation of essentially non-oscillatory shock capturing schemes, II, *J. Comput. Phys*. **83**, 32 (1989).
27. J. L. Steger and R. F. Warming, Flux vector splitting of the inviscid gasdynamic equations with application to finite difference methods, *J. Comput. Phys*. **40**, 263 (1981).
28. J. Thomas and M. Salas, Far-field boundary conditions for transonic lifting solutions to the Euler equations, *AIAA J*. **24**, 1074 (1986).
29. B. van Leer, Flux vector splitting for the Euler equations, in *Lecture Notes in Physics* (Springer-Verlag, New York, 1981), Vol. 170, p. 354.
30. B. van Leer, Towards the ultimate conservative difference scheme. III. Upstream-centered finite-difference schemes for ideal compressible flows, *J. Comput. Phys*. **23**, 263 (1977).
31. V. Venkatakrishnan, Convergence to steady state solutions of the Euler equations on unstructured grids with limiters, *J. Comput. Phys*. **118**, 120 (1995).
32. P. Woodward and P. Colella, The numerical simulation of two dimensional fluid flow with strong shocks, *J. Comput. Phys*. **54**, 115 (1984).